Conformal Magnifier: A Focus+Context Technique with Local Shape Preservation

Xin Zhao, Wei Zeng, *Member*, *IEEE*, Xianfeng David Gu, *Member*, *IEEE*, Arie E. Kaufman, *Fellow*, *IEEE*, Wei Xu, and Klaus Mueller, *Senior Member*, *IEEE*

Abstract—We present the conformal magnifier, a novel interactive focus+context visualization technique that magnifies a region of interest (ROI) using conformal mapping. Our framework supports the arbitrary shape design of magnifiers for the user to enlarge the ROI while globally deforming the context region without any cropping. By using the mathematically well-defined conformal mapping theory and algorithm, the ROI is magnified with local shape preservation (angle distortion minimization), while the transition area between the focus and context regions is deformed smoothly and continuously. After the selection of a specified magnifier shape, our system can automatically magnify the ROI in real time with full resolution even for large volumetric data sets. These properties are important for many visualization applications, especially for the computer aided detection and diagnosis (CAD). Our framework is suitable for diverse applications, including the map visualization, and volumetric visualization. Experimental results demonstrate the effectiveness, robustness, and efficiency of our framework.

Index Terms—Conformal mapping, focus+contex visualization, magnifier shape, smooth deformation, local shape preservation

1 Introduction

With the tremendous increases in computing power, data storage, and internet bandwidth, we can now easily store, process, and deliver over the internet very large data sets, but an inherent limitation is the real estate available to display these data. While display devices may have grown in size and resolution, a natural limit is and remains to be the human's visual field of view. At the same time, with the emergence of portable devices, such as netbooks and smart phones, there has also been a reverse trend in screen size for mobile applications. Therefore, no matter what display size is being used, a careful management of the display real estate is directly required. A natural solution to these requirements is focus+context (F+C) visualization. It allows the users to grasp the overall theme of the data to guide the sense-making process, while allowing them to access and address the appropriate detail of interest. Many F+C techniques have become available in recent years. As a general rule, a good F+C method must support continuity when transitioning from the magnified to the minified areas. Only then can the user perform effective visual searches at these multiple levels of scales. Such transitions are natural to humans because they match their biological visual system where peripheral vision has less detail than the retinal areas closer to the *fovea centralis*. Optical lenses have been available for centuries and humans have become very familiar with them. Computers can easily simulate lenses' effects, while at the same time providing great opportunity to overcome limitations of lenses.

Our paper addresses a specific limitation that optical lenses as well as their many digital counterparts have: their local distortion. Since humans have become accustomed to lens distortions over centuries, they have accepted them and even mentally compensated for their limitations. For example, the surgeon performing minimally invasive endoscopic procedures is aided by lens devices every day. He mentally unwarps the presented imagery without problems. However, when features become sufficiently intricate, and when motion parallax is missing as in static presentational views then lens distortions are intolerable. Therefore, a new lens with local shape preservation is required even for experienced doctors to support accurate detection and diagnosis. Although current lenses are "magic" in the sense what they can reveal, they are less so when it comes to overcoming serious distortion effects or artifacts. We address here the specific need to control local distortion, to preserve local detail undistorted and thus enable the user to reliably read and decode accurate information.

Our lens uses the concept of *conformal mapping* as a novel F+C technique to capture the region of interest (ROI) into a single view while providing a smooth transition between the focus and context regions. Instead of only using lenses with regular circle or square shape, arbitrary shape models are embedded in our system to magnify ROIs with different shapes. Our system has a suite of 1D and 2D transfer functions allowing the enhancement and selection of areas and features of interest, and further interacts with 2D or 3D visual presentations of the data set directly and displays the magnification results in real time. Consequently, our technique has a wide range of application areas, even on smart phones as well as web browsers.

Distortion is also a key factor to improve the visual ability. The improper magnification distortion may cause

- *The authors are with the Computer Science Department, Stony Brook University, Stony Brook, NY 11794-4400.*
E-mail: {xinzhao, zengwei, gu, ari, wxu, mueller}@cs.sunysb.edu.

Manuscript received 3 Jan. 2011; revised 24 June 2011; accepted 1 Feb. 2012; published online 29 Feb. 2012.
Recommended for acceptance by H.-W. Shen.
For information on obtaining reprints of this article, please send e-mail to: tvcg@computer.org, and reference IEEECS Log Number TVCG-2011-01-0001.
Digital Object Identifier no. 10.1109/TVCG.2012.70.

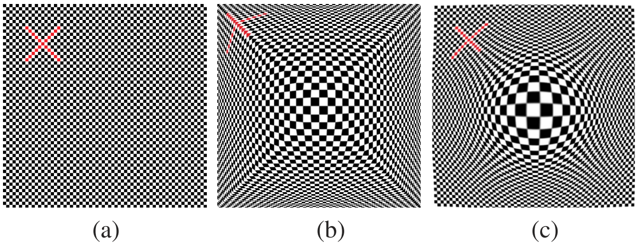

Fig. 1. Basic merits of our conformal mapping compared with the traditional lens for symbols located in the transition region between the focus and context regions. (a) A checker board image with a red X-like symbol. Magnification results using (b) the fisheye lens and (c) our conformal magnifier.

cognition confusion. Any gain from integrating the detail with the surrounding context may easily be lost if the transition between the focus and context regions is difficult to understand. Our *conformal magnifier* minimizes global angle distortions and preserves local angular relationships which, in turn, preserve important shapes and features of objects during the deformation. According to the research result presented by Hong et al. [18], the local angle of objects is an important structure-based factor/descriptor for the visual cognition. This property plays a crucial role during the magnification, especially in the transition region between the focus and context areas, as shown in Fig. 1. After the magnification, the test symbol is hard to be identified and recognized visually by the traditional fisheye lens because of its local angle and area distortion in the transition area, while our conformal magnifier well preserves the local orthogonal features of the symbol. Although the area of the symbol of interest is distorted during the magnification, with the local angle/shape preservation, the recognition of the focus object and its context is relatively straightforward to the user. We are specifically interested in this angle preserving method, especially for the computer aided detection (CAD), because the 3D geometric features are carried by the mapping with high fidelity. For example, Fig. 7 illustrates a premarked polyp on a colon surface both in original 3D view and in display view of our system. It is obvious that the shape of the polyp is well preserved after the magnification. During the diagnosis, radiologists identify colon polyps mainly based on shape information.

Our method is advantageous over previous approaches, as the application of the conformal magnifier well preserves the local shape feature, keeps the global structure, and builds a smooth transition field, leading to reliable zooming results.

The main contributions of our paper are:

- Arbitrary shape models, used as magnifiers to satisfy different application needs.
- A conformal magnifier with local shape preservation and smooth transition.
- The general applicability of our framework for diverse graphics and visualization areas.

To the best of our knowledge, no previous work has used conformal mapping theory as an F+C technique for visualization. In this respect, our conformal magnifier, representing an ideal continuous multifocus F+C technique that we have augmented with several unique features, is a novel nonlinear magnification method. The well-defined conformal function is numerically well behaved: in theory, conformal mapping does not have any local angle distortion. Namely, everywhere, there is neither angle nor shape distortion. In the discrete setting of triangular meshing structure, the approximation of conformal mapping globally minimizes the angle distortion. Therefore, conformal mapping is able to well preserve both local and global shapes with minimal distortion, robustly supporting the solution of several challenging cases.

Our paper is structured as follows: first, in Section 2, we present the overview of related work. Then, in Section 3, we propose our framework and its theory, method, and design in detail. Next, in Section 4, we describe the implementation details. Finally, we show the results for various cases, and demonstrate the merits of our framework in Section 5. Section 6 ends with conclusions and discusses the limitation and future work.

2 Related Work

F+C visualization has been addressed in a great number of papers, including trees [27], [34], treemaps [12], [22], graphs [14], [26], tables [39], city and maps [7], nested networks [41], and 3D models [44], especially for medical data [10]. The commonly used F+C techniques are lenses and magnifiers, such as fisheye [13], nonlinear magnification transformation [23], detail-in-context [21], distortion [25], multiscale [7] and others. Fisheye lenses offer an effective navigation and browsing device for various applications [33]. InterRing [46] and Sunburst [37] have applied multifocus fisheye techniques as an important feature for radial space-filling hierarchical visualizations. The fisheye lens displays the data in a continuous manner, having an advantage in the spatial relation preservation. However, it creates noticeable distortions toward its edges and has no method to formally control the focus region as well as to preserve local features in the context region. Our method, taking the merit of the fisheye lens, continuously preserves the spatial relation, and does a better job in minimizing the distortion and formally controlling the focus region.

Many sophisticated lenses and new distortion techniques have been proposed to enhance the F+C visualization. Spence and Apperley [35] have first simulated the display of the bifocal lens and applied it for various applications. Bier et al. [2] have presented a user interface that enhances the focal features of interest and compresses the less interesting regions using a Toolglass and Magic Lenses. Carpendale et al. [4] have proposed several view-dependent distortion patterns to visualize the internal ROI, and a framework for unifying presentation space to make effective use of the available display space [6]. LaMar et al. [24] have presented a magnification lens with a tessellated border region according to the radius of lenses and the texture information. Pietriga and Appert [28] have provided a novel sigma lens using time and translucency to achieve more efficient transitions, and have also proposed an in-place magnification and representation-independent system that can be implemented with minimal effort in different graphics frameworks [29]. However, all the above methods either remove part of the context areas or seriously distort the transition region: each of them limits the spatial readability, visibility, and continuity for most applications. The smooth transition design between the focus and context regions can preserve the visual continuity and stability, and then effectively increase the visual perception. Our magnifier, based on the strict mathematical solution of conformal mapping, generates a smooth and continuous transition area without losing any context information for the visual consistency.

City and route F+C visualization is another popular application. For the virtual city, Qu et al. [30] have described an F+C route zoom and information overlay method for 3D urban environments. Trapp et al. [42] have proposed a 3D generalization lens for the interactive F+C visualization and applied it to virtual city models with different levels of structural abstraction. For the viewing of routes, Ziegler and Keim [48] have presented an automated system for generating context-preserving route maps. It depicts navigation and orientation routes as a path between nodes and edges of a topographic network. Recently, Karnick et al. [20] have presented a novel multifocus technique to generate a printable version of a route map that shows the overview and detail views of the route within a single, consistent visual frame. These methods, however, may fail to preserve either the local features or the overall context of the surrounding map constituents, such as nearby cities, forests, and other useful information. Our method magnifies the target routes with local shape preservation while keeping all context information.

For the F+C visualization of 3D data, deformation methods have been widely used. For volumetric data, Wang et al. [43] have proposed a free-form volumetric lens function to highlight, expose, and nonlinearly magnify the target. However, the serious context distortion and the deformed transition are major problems neglected by their method, which significantly lower the accurate understanding because of the loss of continuous viewing. For large surface models, Wang et al. [44] have presented an energy optimization model for magnifying ROIs while deforming the context area. Later, they further applied their model to the volumetric data sets to preserve features of interest in F+C visualizations [45]. However, the distortion mechanism of Wang's system is highly arbitrary and determined by the location/distribution of features. By comparison, our conformal mapping, with a clear data-independent distortion, will always behave the same way, no matter what the density or structure of the data is. Moreover, as mentioned in both papers [44], [45], their mechanism fails to preserve the global scale. However, our conformal magnifier, applied for both volumetric data sets and surface mesh models, is specially designed to eliminate the local angle distortion and to preserve the visual continuity in a consistent and global way (e.g., a foot data set in Fig. 8). From the perspective of quality of magnification results, instead of using uniform grid cubes with the number of 20^3 or less proposed by Wang et al. [44], our method is voxel oriented with full resolution (at least 64^3), performed in real time. In practice, partitioning the model with a finer grid space (especially for complex models) will lead to better results but significantly increase the computation cost [44]. Therefore, in terms of computing speed, our system is at least 10 times faster in rendering the F+C display of various large volumetric data sets (details in Section 4.2), thanks to the precomputed intrinsic conformal parameters and the efficient mapping algorithm.

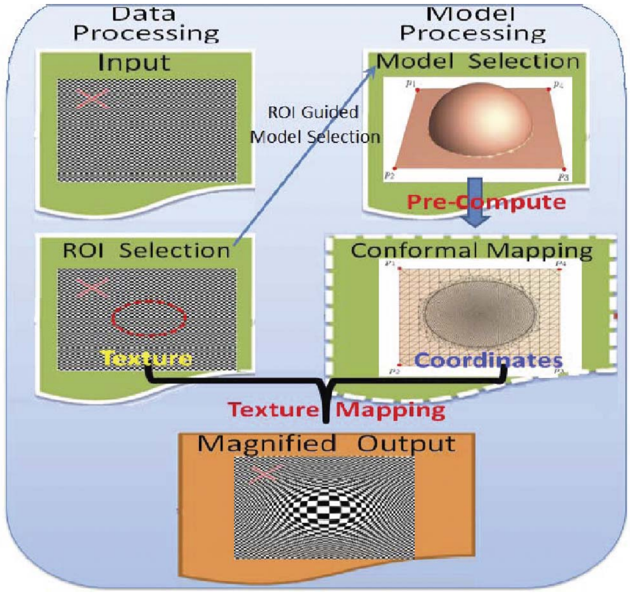

Fig. 2. A schematic diagram of our conformal magnifier pipeline using a simple 2D checker board image as input.

In mathematical theory, different from various lenses that are based on the optical projection and reflection system [3], [47], the core idea of our method is the well-known conformal mapping theory, which is a mathematically rigorous method and one of the best solutions to obtain an optimal angle preservation. Our conformal magnifier well preserves the local features and builds a smooth transition between the focus and context regions by solving the self-contained conformal mapping equations, leading to reliable magnification results. The conformal mapping theory also enables the user to design *arbitrary* shape magnifier models to effectively cover the entire ROI without panning the magnifier around or enlarging non-interest regions (e.g., a route view in Fig. 12). Meanwhile, our system can be easily and directly extended for various applications, ranging from 2D multiscale images to 3D time-series data sets.

3 Conformal Magnifier

Our conformal magnifier is built upon the conformal mapping theory. Fig. 2 shows the pipeline of our framework. There are two precomputation steps: magnifier mesh model design and conformal mapping. An arbitrary mesh model as the magnifier can either be automatically generated based on mathematical definitions or be manually drawn through the user interface. Then, our system precalculates the conformal map of each magnifier model (parameterization of each vertex of mesh model). For any input, including both 2D map and 3D volumetric data sets, with the user-defined ROI and magnifier models, our system can automatically display magnification results in real time using texture mapping or volume rendering. In this section, we first introduce the magnifier mesh model design, and then briefly describe the theory and algorithm of conformal mapping.

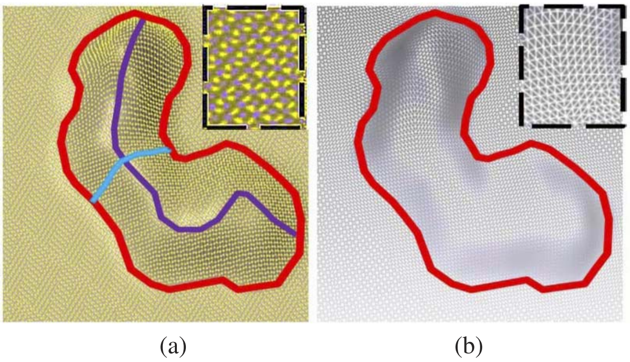

Fig. 3. Two steps in designing a magnifier model with an arbitrary shape: (a) Point cloud generation with respect to the user-defined (red) boundary and (purple) centerline. The cyan line is a quadratic curve for generating 3D interpolation points between a boundary sample point and its nearest centerline sample point. (b) Mesh model generation using the point cloud generated in (a). The black dashed boxes show the magnified details.

3.1 Magnifier Model Design

Basic interactive operations, such as setting and adjusting, can be used to generate an arbitrary model. However, the implementation of these operations is complicated and time consuming for complex models. Therefore, we propose an alternative method for the arbitrary magnifier model design with two steps: point cloud construction and mesh generation from point cloud, as shown in Fig. 3.

Point cloud construction. The specified plane point cloud is constructed by the boundary curve and centerline drawn by the user to highlight the ROI, as shown in Fig. 3a. The user can adjust the magnification ratio by adjusting the height of the centerline along z-direction position (in R^3 with P_{xy} as a 2D plane). Then, the system automatically discretizes both boundary curve and centerline based on the sampling rate. For each boundary sample point, the L2-nearest centerline sample point is found to form a pair. For each pair, a predefined quadratic function (e.g., Gaussian function) is set with the current pair as start and end points, and then the interpolated positions of new cloud points are calculated and generated based on it, which results in a model (for the entire plane) with a continuous and smooth transition. The sampling rate can be interactively set by the user. In general, a high sampling rate generates a large number of points and fits the transition area smoothly, but takes long to compute (e.g., 14.36 second for a test point cloud with 20,152 points).

Mesh generation from point cloud. We generate smooth surface meshes from the point cloud based on Delaunay refinement [31]. First, we find the constrained Delaunay triangulation of the input vertices. Next, we remove triangles from concavity and hole structures. We can further refine the mesh by inserting additional vertices if necessary. This algorithm generates a smooth mesh surface and guarantees the accuracy of the surface approximation, as shown in Fig. 3b. The manifold extraction is also implemented to have a regular smooth surface using the ball pivoting method [1]. In practice, more points in high curvature features produce a better fitting surface. The computation speed of the mesh generation is mainly affected by the number of points, and the shape and topology of the point cloud (e.g., 24.77 second for the same test point cloud with 20,152 points).

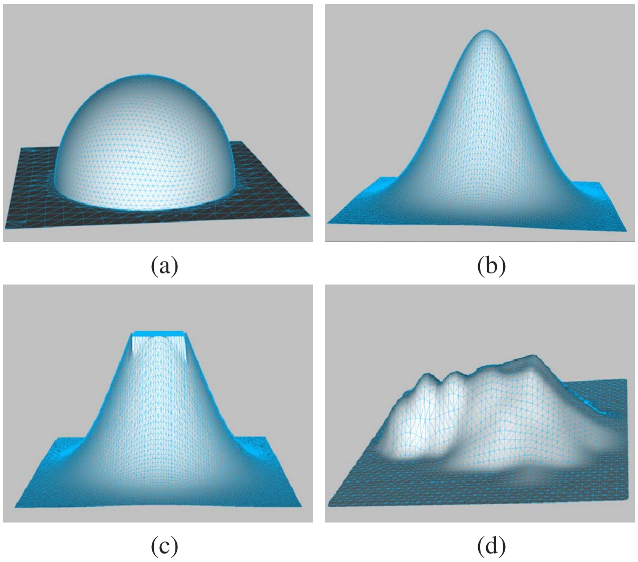

Fig. 4. Various specified mesh models. Regular shapes using (a) a hemisphere and (b) a Gaussian function. Arbitrary shapes using (c) a square plane with a smooth Gaussian transition, and (d) a random shape. The height of each model is nonlinearly proportional to its magnification ratio.

With this design method, the user can interactively define various regular or specified magnifier models (Fig. 4) to magnify the ROI. Different from traditional lens design methods, where each lens must have a specified optical model or an explicit function definition for the ROI magnification, our framework supports any shape or topology magnifier model without a simple explicit/implicit function definition or even without any mathematical description. Supported by conformal mapping theory, the *truly* arbitrary magnifier model design is the first major advantage of our framework.

3.2 Conformal Mapping Theory

After the model generation, the next step is the conformal parameterization for each magnifier model. In this section, we present the merits of conformal mapping and briefly introduce the basic theory background of conformal geometry, necessary for the discussion in this work. For more details, we refer readers to [11] for Riemann surface theory and [16] for differential geometry.

3.2.1 Merits of Conformal Mapping

In general, conformal mapping has its special properties, which are extremely valuable for real applications:

Angle preserving. Conformal mappings are angle preserving. The most common examples of conformal mappings are univalent analytical functions in complex analysis. A more general definition is given in differential geometry [16]. Intuitively, suppose $f: S_1 \to S_2$ is a mapping between two surfaces S_1, S_2, and $\gamma_1, \gamma_2 \subset S_1$ are two arbitrary intersecting curves on S_1, with the intersection point as $p = \gamma_1 \cap \gamma_2$. Then they are mapping to intersecting curves on S_2, $f(p) = f(\gamma_1) \cap f(\gamma_2)$. Suppose at the intersection point p, the intersection angle between two tangent vectors $d\gamma_1, d\gamma_2$ is θ. f is conformal, if and only if the intersection angle between the tangent vectors $df(\gamma_1)$ and $df(\gamma_2)$ is also θ. A formal definition is as follows: $f : (S_1, \mathbf{g}_1) \to (S_2, \mathbf{g}_2)$ is conformal, where $\mathbf{g}_k$ is the Riemannian metric on S_k, $k = 1, 2$, if and only if

$$f^*\mathbf{g}_2 = e^{2\lambda}\mathbf{g}_1,$$

where $\lambda : S_1 \to \mathbb{R}$ is a function, $f^*\mathbf{g}_2$ is the pull back metric induced by f on S_1. Namely, locally a conformal mapping is a scaling transformation, $e^{2\lambda}$ is the scaling factor, therefore it is *shape preserving*.

Intrinsic. Conformal parameterization of a surface is solely determined by its Riemannian metric and does not require its embedding in $\mathbb{R}^3$. For example, one can change a magnifier model by rotation, translation, folding, and bending without stretching, the conformal parameterization is invariant.

Stable and Practical. Computing conformal parameterization is equivalent to solving an elliptic geometric PDE [32], which is stable and insensitive to the noise and the resolution of the data. Therefore, a low-resolution magnifier (around 3K vertices) is good enough for most cases. It also effectively accelerates the computation of conformal mapping.

3.2.2 Conformal Structure

Conformal structure and its properties are important mathematical foundations used to support our solid conformal mapping theory. Thus, in this section, we briefly introduce the necessary background knowledge of conformal geometry.

Suppose S is a surface embedded in $\mathbb{R}^3$, therefore S has the induced euclidean metric $\mathbf{g}$. Let $U_\alpha \subset S$ be an open set on S, with local parameterization $\phi_\alpha : U_\alpha \to \mathbb{C}$, such that the metric has local representation

$$\mathbf{g} = e^{2\lambda(p)} dz d\bar{z}, \quad p \in U_\alpha,$$

where $\lambda : U_\alpha \to \mathbb{R}$ is called a *conformal factor* function, $z \in \mathbb{C}$ is parameter coordinates, d denotes the exterior derivative. Then (U_α, ϕ_α) is called an *isothermal coordinate chart*. The whole surface can be covered by a collection of isothermal coordinate charts. All the isothermal coordinate charts form a *conformal structure* of the surface. The surface with a conformal structure is a *Riemann surface* [11]. Suppose S_1 and S_2 are two Riemannian surfaces. Suppose (U_α, ϕ_α) is a local chart of S_1, (V_β, ψ_β) is a local chart of S_2. $\phi : S_1 \to S_2$ is a *conformal map* if and only if

$$f = \psi_\beta \circ \phi \circ \phi_\alpha^{-1} : \phi_\alpha(U_\alpha) \to \psi_\beta(V_\beta),$$

is biholomorphic, i.e., it satisfies the Cauchy-Riemann equation $\frac{\partial f}{\partial \bar{z}} = 0$. For simplicity, we still use ϕ to denote its local representation. Then a conformal map ϕ satisfies $\frac{\partial \phi}{\partial \bar{z}} = 0$.

3.2.3 Conformal Mapping by Surface Ricci Flow

Let S be a surface embedded in $\mathbb{R}^3$ with the induced euclidean metric $\mathbf{g}$. We say that another Riemannian metric $\bar{\mathbf{g}}$ is *conformal* to $\mathbf{g}$, if there is a scalar function $u : S \to \mathbb{R}$, such that $\bar{\mathbf{g}} = e^{2u}\mathbf{g}$. The Gaussian curvature induced by $\bar{\mathbf{g}}$ is

$$\bar{K} = e^{-2u}(-\Delta_{\mathbf{g}} u + K),$$

where $\Delta_{\mathbf{g}} = e^{-2\lambda}(\frac{\partial^2}{\partial x^2} + \frac{\partial^2}{\partial y^2})$ is the Laplacian-Beltrami operator under the original metric $\mathbf{g}$, K the original Gaussian curvature under $\mathbf{g}$, $\bar{K}$ the induced Gaussian curvature under $\bar{\mathbf{g}}$. The above equation is called the *Yamabe equation*. By solving the Yamabe equation, one can design a conformal metric $e^{2u}\mathbf{g}$ by a prescribed target curvature $\bar{K}$.

Ricci flow can be used to solve Yamabe equation. It is a powerful tool which has been used for proving the Poincaré conjecture. Ricci flow behaves like a heat diffusion process in the following form:

$$\frac{dg_{ij}(t)}{dt} = 2(\bar{K} - K(t))g_{ij}(t),$$

where t is the time parameter. If $\bar{K} \equiv 0$, Ricci flow deforms the Riemannian metric $\mathbf{g}$ to the *uniformization metric* $\bar{\mathbf{g}}$ by evolving the Gaussian curvature K, such that the Gaussian curvature becomes constant everywhere, according to the surface uniformization theorem in [11]. The convergency of Ricci flow to the uniformization metric has been proved in [8] and [17]. In this paper, we deal with quadrilateral surfaces with euclidean background geometry, and map them to a planar rectangle parametric domain. Thus, we choose $\bar{K} = 0$ at interior points and $\bar{K} = \pi/2$ at four boundary corners in such cases.

3.2.4 Discrete Surface Ricci Flow

Here we describe several major concepts for computing Ricci flow on discrete surfaces. In practice, most surfaces are approximated by simplicial complexes, namely triangular meshes. Suppose M is a triangle mesh, V, E, F are vertex, edge, and face set, respectively. We use v_i to denote the ith vertex; $[v_i, v_j]$ the edge from v_i to v_j; $[v_i, v_j, v_k]$ the face, where the vertices are sorted counter-clock-wisely.

Discrete metric and curvature. A *discrete metric* on a mesh M is a function $l : E \to \mathbb{R}^+$, such that on each face $[v_i, v_j, v_k]$, the triangle inequality holds, $l_{jk} + l_{ki} > l_{ij}$. If all faces of M are euclidean, then the mesh is with euclidean *background geometry*, denoted as $\mathbb{E}^2$. The discrete metric represents a configuration of edge lengths and determines the corner angles on each face by cosine law,

$$\theta_i^{jk} = \cos^{-1}\frac{l_{ki}^2 + l_{ij}^2 - l_{jk}^2}{2l_{ki}l_{ij}},$$

where θ_i^{jk} is the angle at v_i opposite to edge $[v_j, v_k]$ in the face. The *discrete Gaussian curvature* of v_i is defined as an angle deficit at v_i, considering all the corner angles surrounding a vertex v_i,

$$K_i = \begin{cases} 2\pi - \sum_{jk} \theta_i^{jk}, & v_i \notin \partial M, \\ \pi - \sum_{jk} \theta_i^{jk}, & v_i \in \partial M. \end{cases}$$

Circle packing metric. The discrete Ricci flow can be carried out through the circle packing metric, which is a discretization of conformality and was introduced by Thurston [40]. Each vertex v_i is associated with a circle with radius r_i. Two circles at the end vertices of an edge $[v_i, v_j]$ intersect at an angle θ_{ij}, then the edge length l_{ij} is given by

$$l_{ij}^2 = r_i^2 + r_j^2 + 2r_ir_j\cos\theta_{ij}.$$

A conformal deformation maps infinitesimal circles to infinitesimal circles and preserves the intersection angles

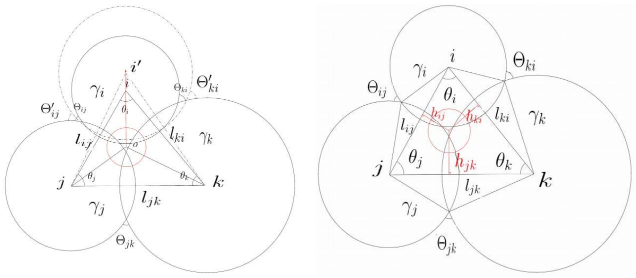

(a) (b)

Fig. 5. Geometric interpretation of discrete conformal metric deformation. (a) Conformal circle packing metric deformation and (b) the radial circle (in red) of a triangle.

among the infinitesimal circles. As shown in Fig. 5a, the circle radius centered at each vertex deforms while not changing the intersection angles among circles $\theta'_{ij} = \theta_{ij}$, $\theta'_{ik} = \theta_{ik}$. The circle packing metric can be defined as $\mathbf{u} = \{u_i\}$, where $u_i = \log r_i$, r_i is the circle radius of v_i. The variation of the circle packing metric under Ricci flow generates the desired metric.

Discrete conformal metric deformation. We apply the discrete Ricci flow method to conformally map the surfaces onto planar domains $\phi : M \to D$. In all configurations, the discrete Ricci flow is defined as follows:

$$\frac{du_i(t)}{dt} = \bar{K}_i - K_i, \tag{1}$$

where $\bar{K}_i$ is the user-prescribed target curvature and K_i is the curvature induced by the current metric. The discrete Ricci flow has exactly the same form as the smooth Ricci flow, which conformally deforms the discrete metric according to the Gaussian curvature.

The discrete Ricci flow can be formulated in the variational setting, namely, it is a negative gradient flow of a special energy form, called *Ricci energy*, which is given by

$$f(\mathbf{u}) = \int_{\mathbf{u_0}}^{\mathbf{u}} \sum_{i=1}^{n} (\bar{K}_i - K_i) du_i, \tag{2}$$

where $\mathbf{u_0}$ is an arbitrary initial metric. Computing the desired metric with user-defined curvature $\{\bar{K}_i\}$ is equivalent to minimizing the discrete Ricci energy.

The Hessian matrix for discrete Ricci energy is positive definite for the euclidean case (with normalization constraint $\sum_i u_i = 0$). Therefore, the energy is convex and can be optimized using Newton's method. The Hessian matrix is computed on the circle packing metric [40]. As shown in Fig. 5b, the *radial circle* of a triangle is unique and perpendicular to each vertex circle. For all configurations with euclidean metric, suppose the distance from the radial circle center to edge $[v_i, v_j]$ is d_{ij}, then $\frac{\partial \theta_i}{\partial u_j} = \frac{d_{ij}}{l_{ij}}$, furthermore, $\frac{\partial \theta_j}{\partial u_i} = \frac{\partial \theta_i}{\partial u_j}, \frac{\partial \theta_i}{\partial u_i} = -\frac{\partial \theta_i}{\partial u_j} - \frac{\partial \theta_i}{\partial u_k}$. We define the edge weight w_{ij} for edge $[v_i, v_j]$ which is adjacent to triangles $[v_i, v_j, v_k]$ and $[v_j, v_i, v_l]$ as

$$w_{ij} = \frac{d_{ij}^k + d_{ij}^l}{l_{ij}}.$$

The Hessian matrix $\mathbf{H} = (h_{ij})$ is given by the discrete Laplace form,

$$h_{ij} = \begin{cases} 0, & [v_i, v_j] \notin E, \\ -w_{ij}, & i \neq j, \\ \sum_k w_{ik}, & i = j. \end{cases}$$

According to the Gauss-Bonnet theory [16], the total curvature must be $2\pi\chi(M)$, where χ is the Euler characteristic number of M. In our application, M is a topological quadrilateral, so $\chi(M) = 1$. We set the target curvature of the four boundary corners to be $\pi/2$, other boundary vertices and interior vertices to be 0. Then the topological quadrilateral is mapped to a rectangle. The convergency of discrete Ricci flow has been proved by [9]. Details about discrete analog for general Ricci flow can be found in [15] and [19].

3.3 Conformal Mapping Algorithm

The discrete Ricci energy can be optimized using Newton's method to achieve the unique global optimal metric with the prescribed curvature. The implementation detail is listed in Algorithm 1.

Algorithm 1. Newton's Method of Discrete Ricci Flow
Input: A 3D mesh $M = (V, E, F)$, target curvature $\bar{\mathbf{K}} = \{\bar{K}_i\}$, curvature error threshold ε.
Output: Corresponding 2D parameterization positions u of mesh vertices, used as coordinates for texture mapping or volume rendering.
Initial the parameterization position u_0 and curvature $\mathbf{K} = \{K_i\}$
while $\max|K_i - \overline{K}_i| > \varepsilon$ **do**
  for all edges $e = [v_i, v_j] \in E$ **do**
    $l_{ij} \leftarrow \sqrt{\gamma_i^2 + \gamma_j^2 + 2\gamma_i\gamma_j \cos\theta_{ij}}$ {Compute the edge length by radii γ_i, γ_j centered at v_i, v_j}
  end for
  for all corner angles $\theta_i \in [v_i, v_j, v_k]$ **do**
    $\theta_i \leftarrow \cos^{-1} \frac{l_{ij}^2 + l_{ki}^2 - l_{jk}^2}{2 l_{ij} l_{ik}}$ {Compute the corner angle}
  end for
  for all edges $e = [v_i, v_j] \in E$ **do**
    $w_{ij} \leftarrow \frac{d_{ij}^k + d_{ij}^l}{l_{ij}}$ {Compute the edge weight}
  end for
  for all vertices $v_i \in V$ **do**
    $h_{ij} \leftarrow -w_{ij}, [v_i, v_j] \notin E$;
    $h_{ii} \leftarrow \sum_k w_{ik}$ {Compute the Hessian matrix $\mathbf{H}$}
  end for
  $d\mathbf{u} \leftarrow \mathbf{H}^{-1}(\mathbf{K} - \bar{\mathbf{K}})$ {Minimize the discrete Ricci energy}
  for all vertices $v_i \in V$ **do**
    $u_i \leftarrow u_i + du_i$ {Update the circle packing metric for the calculation of each corresponding parameter position}
  end for
  for all vertices $v_i \in V$ **do**
    $K_i \leftarrow 2\pi - \sum_{jk} \theta_i^{jk}, v_i \notin \partial V$; or
    $K_i \leftarrow \pi - \sum_{jk} \theta_i^{jk}, v_i \in \partial V$ {Update the Gaussian curva ture}
  end for
end while

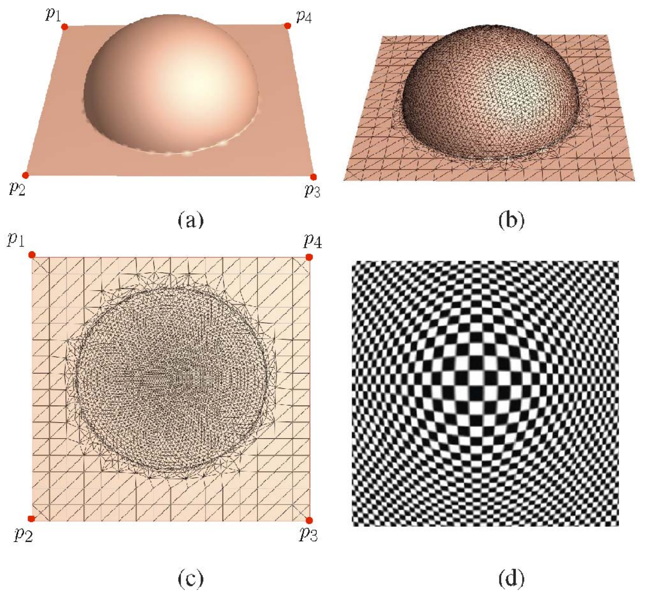

Fig. 6. Conformal mapping for a topological quadrilateral surface: (a) The original surface. (b) The corresponding triangular mesh magnifier model. (c) The image of the conformal map, which is a rectangle. (d) A checker board texture mapping through the rectangular conformal map, demonstrating that the local angles are correctly preserved.

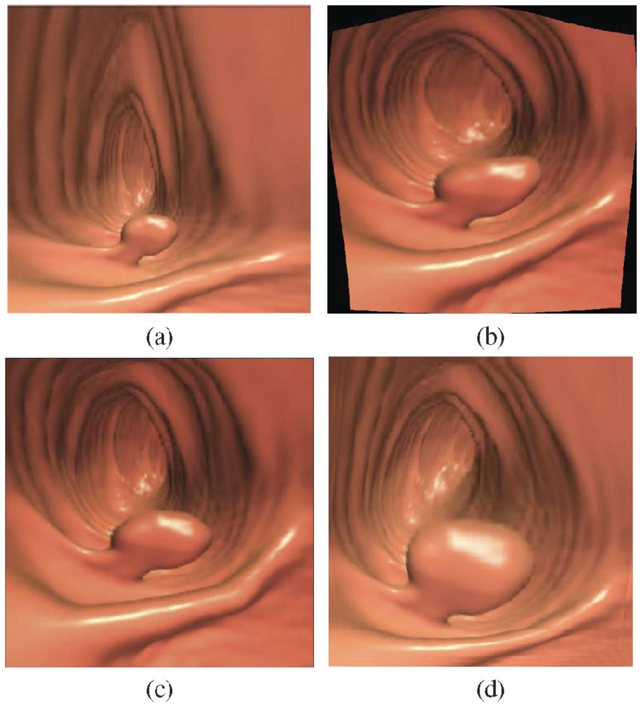

Fig. 7. Magnification results using different lenses for the volumetric colon data set. (a) Original colon data set. Magnification results using the polyfocus lens (b) without and (c) with fixed boundary, following the Carpendale's paper [4]. (d) The magnification result using our conformal magnifier with a Gaussian model: the local shape/features of the interior surface and the polyp are well preserved with the smoothest transition region.

We design the magnifier model as a 2.5D mesh with coordinates (x, y, z) where the model can be projected to the 2D plane with coordinates (x, y), z describes the height from the plane. According to the conformal mapping theory, the local magnification ratio of the conformal magnifier is nonlinearly proportional to the height z at the corresponding vertex $v = (x, y, z)$. Therefore, the global/local magnification ratio is controllable by adjusting the heights of all/some of vertices. The entire computational process for a magnifier model which is a topological quadrilateral is illustrated in Fig. 6. The original magnifier mesh model is shown in Fig. 6a, with four corner vertices noted as p_1, p_2, p_3, p_4. For solving Eqn. 3.2.3, we set the target curvature for each vertex in the triangle mesh (Fig. 6b). The four corner vertices are assigned $\pi/2$, while other vertices are 0. In Fig. 6c, the Ricci flow conformally maps the mesh model onto a planar rectangle, with the corner vertices mapped to the rectangle corners. Thus, we have the conformal map, with the corresponding 2D parameterization position of each vertex in the selected mesh model, used as coordinates for texture mapping or volume rendering. Giving rise to the conformally bijective mapping from checker-board texture to this model-based conformal map in the parameter domain, the ROI is magnified with a smooth transition, as shown in Fig. 6d.

Computing conformal mapping by Ricci flow equals to solving a nonlinear geometric PDE, which is stable and robust to the resolution of models. With an accelerated CPU/GPU solution, the conformal mapping of magnifier models is on second level for most cases (note that the conformal mapping for the designed modelscan is computed *offline*, separated from the F+C magnifying procedure in practice). The *real-time* performance of F+C conformal magnifiers depends on the efficiency of rendering or ray-tracing technique design, which could be easily satisfied on either desktops, netbooks, or smart phones (details in Section 4.2).

Case studies. Based on conformal mapping theory and its algorithmic framework, our conformal magnifier offers mathematical guarantees to achieve a smooth and continuous F+C visualization with local shape preservation. We further demonstrate this merit using comparisons of different lenses with the volumetric colon data set. As shown in Fig. 7b, a major disadvantage of Carpendale's method [4] is the seriously distorted boundary, which significantly decreases the accuracy of the object shape and affects the visual ability of the user. Fig. 7 c shows that, with the radial Gaussian function (fixed boundary), the surroundings of the focal region are seriously stretched due to the distortion being uniformly distributed on the data set. In contrast, our method minimizes the angle distortion and preserves the shape of local features, as shown in Fig. 7d: the fold and polyp of the colon remain similar to their original shape after the magnification.

As an alternative F+C method, although our method is not distortion-free in the focus area, it has a solid mathematical foundation to preserve both local shape and global structure simultaneously and to produce a smooth transition area without any serious distortion. Both properties are important merits for the accurately visual cognition. Fig. 8 shows another magnification comparison results using two prominent methods with the volumetric foot data set. From the perspective of local shape preservation, as shown in Fig. 8b, Carpendale's method [4] seriously deforms the surrounding transition area (two toe bones

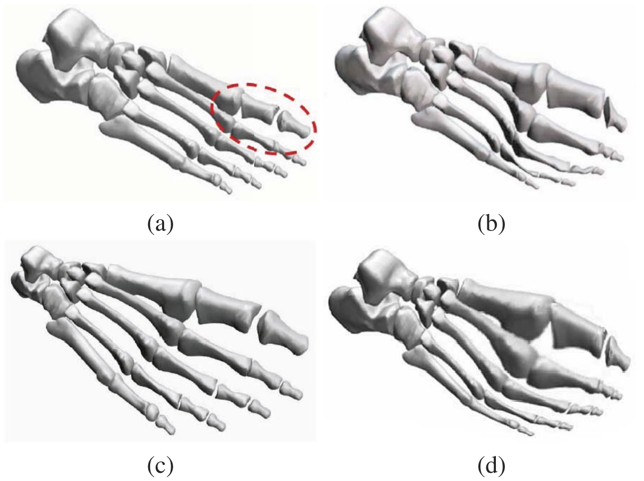

Fig. 8. Magnification results using different lenses for the volumetric foot data set. (a) Original foot surface mesh data set with a predefined focal area (red circle). Magnification results using (b) the polyfocus lens following the Carpendale's paper [4], and (c) the energy-based distortion minimization method [44] (courtesy to Wang et al. [44]). (d) The magnification result using our conformal magnifier with a Gaussian model: both local and global shape/features are well preserved.

near the ROI) without preserving the original shape features. By comparison with the original input data set as shown in Fig. 8a, the magnification results generated by Carpendale's [4] method (Fig. 8b) and our technique (Fig. 8d), respect the global shape/structure of foot data set without any obvious shape confusion for the accurate object recognition. However, as shown in Fig. 8c, after setting the ROI (two foot toes), the magnification result generated by Wang's method [44] well preserves the local structure/shape in the focus area, but seriously affects the context region and introduces visual artifacts for the global structure, such as the extra extension of the left three toes and the overall foot width (the surrounding regions are enforced to expand because the cubes are connected [44]). Wang et al. [44] have also mentioned this problem as one of their major limitations.

4 IMPLEMENTATION

We have implemented a general framework for the conformal mapping-based F+C visualization. Our system is built using a two-tier architecture. The front-end user interface and interactive operations are based on a small number of menu bars, check boxes, and pointer interactions using OpenGL and Glut libraries. There are two modes of the interface: 1) design mode for generating magnifier models, and 2) selection mode for setting ROIs and magnifier models. With the objective to optimize the computing speed, we use the combination of CPU and GPU.

4.1 Precomputation

For efficiency purposes, the core algorithms of our two precomputation steps: mesh generation and conformal mapping, are implemented on the CPU. The computation time of conformal parameterization is proportional to the number of vertices and is slightly affected by the topology shape of each magnifier model. Table 1 shows the model shape, vertex, and face count, and precomputation time of

TABLE 1
Statistics of All Magnifier Models Used in This Paper

Model	No. of Vertices	No. of Faces	Time (s)
Sphere	3446	6826	3.24
Square	3125	6018	3.08
Elongated Model	3691	7063	3.76
Low Gaussian	2192	4830	2.19
High Gaussian	4246	8926	3.97
Curved Model	2639	5328	2.65

conformal parameterization for various magnifier models used in this paper on a Dell desktop precision PWS670 with Intel Xeon CPU 3.60 GHz, 3 GB Memory, and Nvidia GeForce GTX 285 graphic card. Once a magnifier model is parameterized, there is no need to do any parameterization modification for different input data sets. This is the key to the real-time performance of our system.

4.2 Real-Time Performance

We implement the transfer function specification, texture mapping, and volume rendering using GPU acceleration.

4.2.1 *Texture Mapping*

For the 2D texture image, we directly call the texture mapping functions provided by the OpenGL library. Each input image is processed as an 8 bit per-channel texture and directly mapped to the selected magnifier model according to the precalculated conformal parameters. Two interpolation strategies are provided for different input data sets: bilinear interpolation for single image and blending interpolation for multiscale images. The bilinear interpolation is fast and easy-to-implement but without any new detail shown. For the multiscale images, unlike traditional piecewise blending methods in the image domain, supported by the conformal mapping theory, our system directly provides a continuous blending function in the parameter space. Figs. 9b and 9c show the continuous magnification ratios (the continuous parameter distribution) of the hemisphere magnifier model using a color map. They also reveal two properties of conformal mapping: the model height is nonlinearly proportional to the magnification ratio; and the smooth transition of the magnification ratios results from the numerical continuity in the parameter space, which theoretically supports the texture mapping of continuous-scale images. Therefore, the conformally bijective texture mapping between the parameterization value and the image pixel (for both single image and multiscale images) is syntactically and semantically trivial with respect to the user's predefined mapping criteria (e.g., fix the four corner points in Fig. 6). In order to accelerate the search efficiency, we build tree structures for multiscale images with the help of premarked feature points. Take Fig. 9a as an example, the root of a tree structure is a pixel at the largest scale ($100 \text{ km} \times 100 \text{ km}$). Its direct children are right from the next small scale ($10 \text{ km} \times 10 \text{ km}$), and leaves are at the smallest scale ($1 \text{ km} \times 1 \text{ km}$). The smaller scales and leaves contain more details to reveal the local information. We use breadth-first search (BFS) method as a query. In addition,

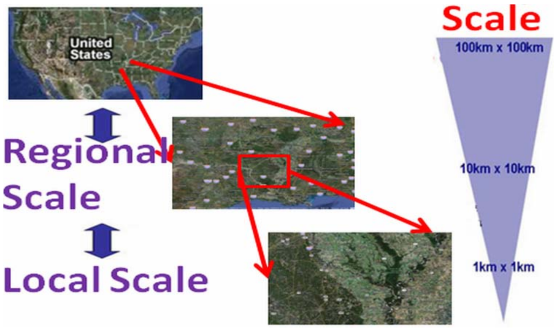

(a)

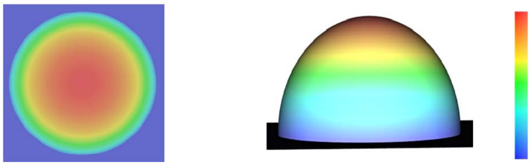

(b) (c)

Fig. 9. Implementation of multiscale magnification using our conformal magnifier with a hemisphere model. (a) Multiscale satellite images of the United States. The ROI contains more details/pixels as the scale decreases (the magnification ratio increases). (b) The top view and (c) the side view of the continuous magnification ratios of our conformal magnifier calculated by conformal mapping. The colorbar shows the scale of the magnification ratio: from large (red) to small (purple).

for the optimal speed and space, we can only search and store tree structures in the ROI.

4.2.2 Volume Rendering

In order to extend the conformal magnifier as a 3D exploration tool, different from the camera texture [36], which locally changes the 2D perspective plane of camera space, we directly replace the 2D camera plane with our 3D magnifier model, as shown in Fig. 10. Fixing a view point, the surface of the 3D hemisphere magnifier model forms a continuous view with the following fact: the closer to the view point, the smaller the view distance will be and the larger the object of interest will be. We adapt the fragment program for volume rendering proposed by Stegmaier et al. [38], considering the model shape and several factors including depth, view angle, and camera position. The steps include, cast the ray into the volume and composite the color based on transfer functions, and render the result to the framebuffer as output. The pixel color and alpha are adjustable by transfer functions. This new rendering method results in a nonlinear magnification of 3D views

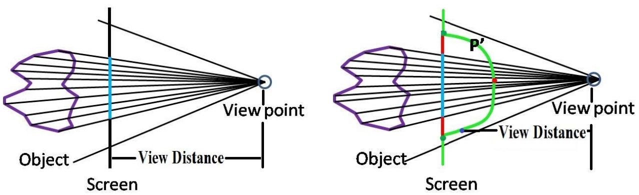

(a) (b)

Fig. 10. The new raycasting scheme: each ray is calculated based on (b) the designed magnifier plane (green curve marked as P') instead of (a) the traditional 2D plane.

TABLE 2
Time Statistics of Texture Mapping or Volume Rendering for All the Data Sets Used in This Paper (f/s: Frames/Second)

Catalog	Name	Size	Model	Time (ms)
Information	Symbol	512^2	Hemisphere	2.6
Route+city	SF city	800×750	Gaussian	3.0
Route+city	Expressway	1080×680	Elongated	3.8
Route+city	NYC	1024^2	Gaussian	4.8
Surface	Foot	vertex:$21.3K$	Gaussian	8.2
Medical	Colon polyps	$512^2 \times 96$	Gaussian	16.3
Medical	Skull	256^3	Gaussian	14.7
Volume	Smoke	64^3	Hemisphere	55 f/s

in real time with less performance degradation. Notice that our method directly works in 3D, which is more realistic and interactive than the direct deformation on the 2D rendered image. In addition, our method is a different approach from some optical 3D lenses (e.g., [43]), as their lenses affect everything in front of the user, but our method could control the shape of distortion region by using different magnifier models.

The texture mapping or volume rendering needs to be recomputed whenever the focus or the magnifier model changes, but with real-time performance. Table 2 shows the texture mapping or volume rendering time for all experimental cases used in this paper on the same desktop mentioned above. The implementation time listed in Table 2 demonstrates that our design strategy is good enough for our purposes: interactive operation of the ROI selection, magnifier model design, and the real-time display.

5 Experimental Results

In this section, we apply our conformal magnifier to various applications and demonstrate the merits of our framework. Because of page limitation, only part of the results are illustrated here, more results are available in the additional electronic materials.

5.1 Route and Map Visualization

Recently, smartphones and notebooks attract increasing attentions, however, the limited input modalities make it difficult to support both clear focus and context regions of large data sets without any extra operation. Our framework improves the magnification function for routes and maps. Our conformal magnifier, as an effective route/map deformation method, overcomes two major shortcomings of Google map: 1) after magnification, the visual consistency is seriously disturbed due to loss of the transition or the context region; and 2) a long trip always requires multiple panning and zooming operations. Fig. 11 shows a magnification result of multiscale maps using our conformal magnifier. With continuous magnification ratios, the result shows multilevel details with a smooth transition between the focus and context regions.

Another advantage of our method is to enable the user to directly design arbitrary magnifier models based on the shape of ROI on the route map. This design has effective merits for the route view: cover the entire ROI without the need of moving the magnifier around, and only cover the ROI without any noninterest region. For example, an

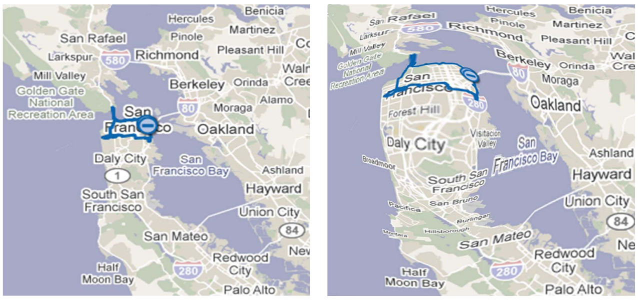

(a) (b)

Fig. 11. Multiscale map magnification results using our conformal magnifier. (a) Original map shows the surrounding region of the city of San Francisco. (b) Two times magnification result shows additional details of the city. The blue line is used to align the multiscale maps. The result also nicely shows that the shape of the blue area is well preserved in the smooth magnification transition area.

elongated magnifier model in Fig. 12b covers the entire route of interest (highlighted by a blue dashed circle), while a regular hemisphere magnifier model in Fig. 12a only covers a small part of it. We define a parameter Λ to describe the ROI magnification efficiency as: $\Lambda = \frac{Area_{ROI}}{Area_{ROM}}$, where ROM is the region of magnification. As shown in Figs. 12a (ROM is highlighted by a blue dashed circle) and 12b, although both magnification results have the high-magnification efficiency ($\Lambda \approx 1.0$), Fig. 12a fails to reveal the entire ROI. If we increase the radius of the hemisphere magnifier model in Fig. 12a (a new ROM is highlighted by a green dashed circle) to cover the entire ROI, many noninterest regions will be magnified as well, sharply decreasing *the magnification efficiency factor* Λ down to 0.63. Our system successfully provides a good magnification scheme for the route view as it presents general route trends and specific spots simultaneously.

In order to further demonstrate the merit of our conformal magnifier for the route and city visualization, popular lenses, including bifocal [35], and fisheye lenses [43], have been implemented as comparison. Fig. 13 shows the route/map magnification results using different lenses. By comparison, our conformal magnifier enlarges the small landmark/roads along the route of interest for a detail view

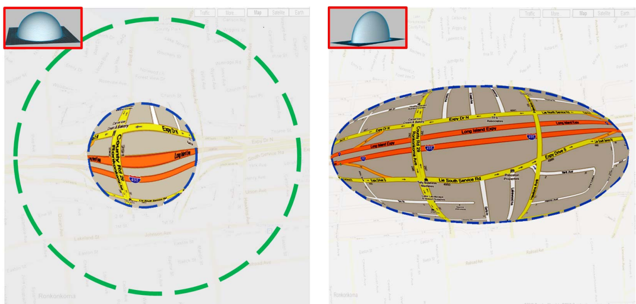

(a) (b)

Fig. 12. Efficient route view using our conformal magnifier. Instead of using (a) hemisphere models with a small (blue dashed circle) and a large radius (green dashed circle), (b) an elongated model can magnify the entire route of interest without taking any extra movement or magnifying any noninterest area. It also has no widening artifacts of the routes of interest.

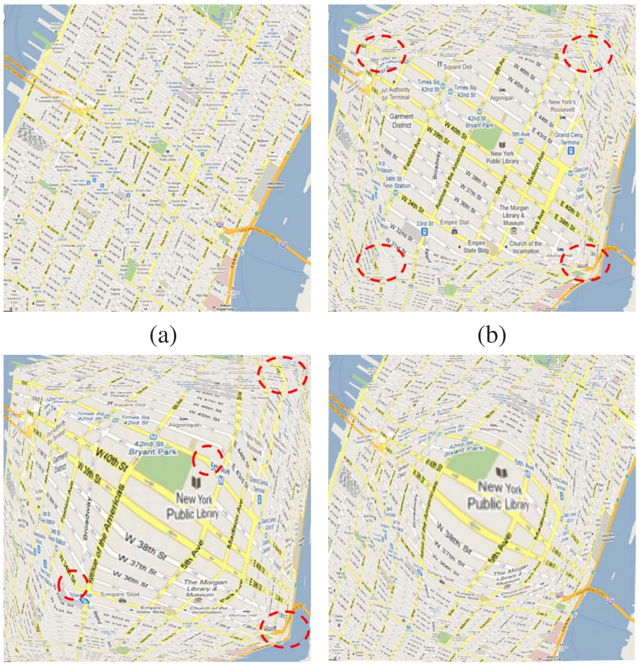

(a) (b) (c) (d)

Fig. 13. Magnification results using different lenses for the NYC street map. (a) Original NYC map. Magnification results using (b) the bifocal lens, (c) the fisheye lens, and (d) our conformal magnifier. The red circles highlight the seriously distorted areas.

with the best local shape preservation, and keeps the entire context region through a smoothest transition.

5.2 Volumetric Data Visualization

Our conformal magnifier can be easily applied to various volumetric data sets for real-time navigation.

Medical data sets. We test our framework using several volumetric medical data sets to demonstrate the advantages of our conformal magnifier: the local shape preservation and smooth transition between the focus and context regions, providing important meanings in clinic education, diagnosis, and virtual surgery. The conformal mapping can be successfully used for the CAD of colon polyps. With its property of shape preservation (angle distortion minimization), doctors can achieve accurate diagnosis since the spherical shape of polyps is a critical feature to distinguish cancer from artifacts. By comparison with traditional lenses, as shown in Fig. 7, both global and local shapes of colon with polyps are well preserved and easily perceived using our conformal magnifier. Fig. 14 shows another medical example. Using our conformal magnifier, although part of the skull area is compressed, each specified local feature of the skull and spine is well preserved in both transition and context regions after the magnification. By comparison, our conformal magnifier has the best magnification result in terms of both shape preservation and smooth transition. These properties are crucial for doctors to learn, detect, and diagnose disease symptoms.

High-level magnification. Our framework can be easily extended to the high-level magnification. The user can interactively reselect ROI and keep on zooming in on the latest magnified result or directly reset the magnification ratio of the magnifier model. Unlike the discrete zooming

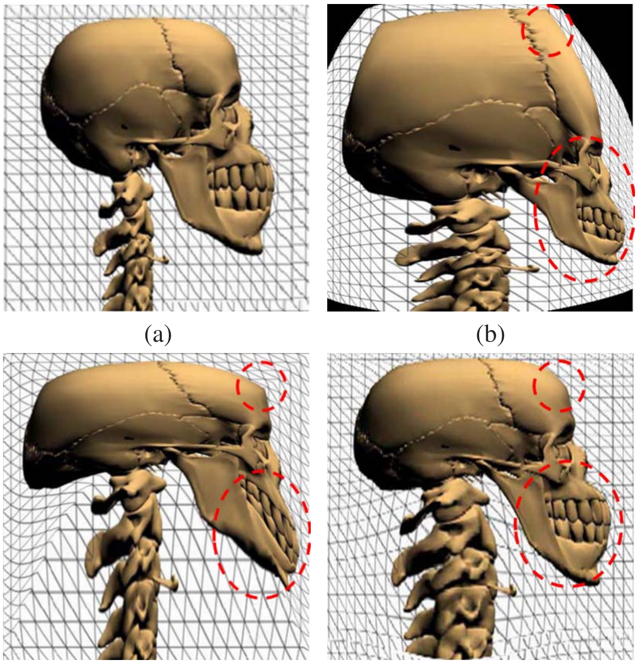

(a) (b)

(c) (d)

Fig. 14. Magnification results using different lenses for the volumetric skull data set. (a) Original human skull data set. The spine is the ROI. Magnification results using (b) the perspective-wall lens, (c) the Carpendale's polyfocus lens with fixed boundary [4], and (d) our conformal magnifier. The background mesh shows the distortion, and the red circles highlight the transition area between the focus and context regions for each method.

factors [5], in theory, our magnifier has continuous magnification ratios to obtain a smooth transition between the focus and context regions during the magnification. In practice, there are no theory or implementation limitations for the design of high-level conformal magnifier. Fig. 15 shows that our conformal magnifier still preserves the local shape details in the ROI (the interior sphere of the smoke data set) and enables a smooth transition after the high-level magnification. However, because of the limitation of the screen real estate, our method may fail to preserve the area of object, which leads to inaccurate measurement. Fortunately, the distorted area and volume information can be reconstructed by referring back to the original volumetric data using the precomputed bijective conformal parameters.

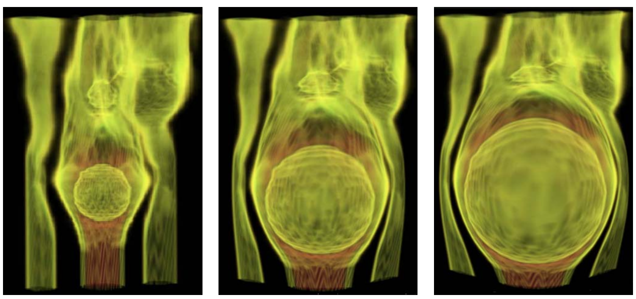

(a) (b) (c)

Fig. 15. High-level conformal magnification results for the volumetric smoke data set. (a) Original smoke data set (b) 9 times and (c) 16 times magnification results.

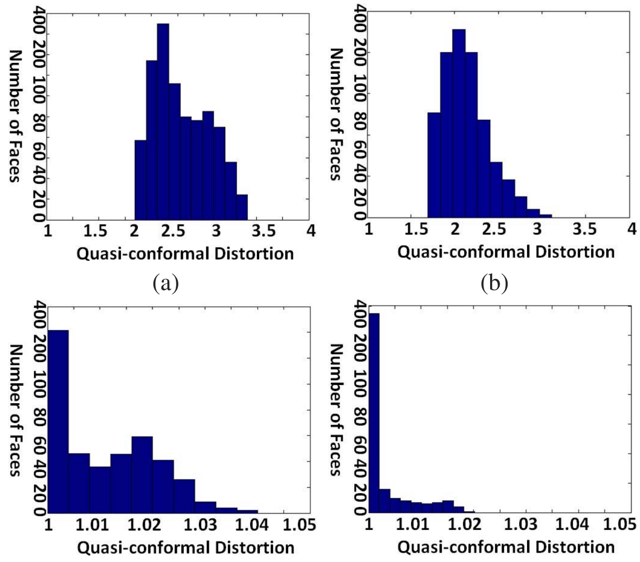

(a) (b)

(c) (d)

Fig. 16. Histograms show the distribution of the quasi-conformal distortion using (a) the fisheye lens, (b) the polyfocus lens following [4], and our conformal magnifiers with (c) a hemisphere model and (d) a Gaussian model.

5.3 Distortion Measurement

In order to quantitatively measure the angle distortions of various lenses, we use *the distortion of conformality*, which is computed as: the ratio of the larger to the smaller eigenvalue of the Jacobian matrix generated using the parameterization value with respect to lens definition functions or magnifier models (details in [11] and [16]). The ideal conformality is 1.0, which is the most conformal. But due to the numerical problem, it cannot be exactly 1.0. The region with a lower distortion value means that it is more similar to its original shape, while the region with a higher distortion value is naturally stretched. We use histograms to show the distribution of *the distortion of conformality* for different lenses. As shown in Figs. 16c and 16d, the mapping of our conformal magnifier is close to conformal everywhere: the maximal errors of our two predefined magnifier models are less than 4 and 2 percent, respectively. By comparison with the fisheye lens (Fig. 16a) and the Carpendale's polyfocus lens [4] (Fig. 16b), our method is statistically significant for the angle preservation (local shape preservation).

6 Conclusions

In this paper, we have presented a simple but powerful conformal magnifier, a conformal mapping-based nonlinear spatial distortion magnifier, as an F+C visualization technique to overcome the limitation of the screen real estate. Our framework focuses on the angle distortion minimization and visual continuity, producing optimally visual results: magnify the ROI with minimal local angle distortion and contain a continuous transition region where the user can get a smooth view from the highly magnified inside to the nonmagnified outside. The properties of local shape preservation and smooth transition have significant applications in many areas, for example, the computer aided detection and diagnosis of diseases, which is always based on the local shape/features and the context information around the focal region. Our system also supports the magnifier model design of arbitrary shapes, enabling an extremely flexible and natural style of direct manipulations for data analysis. In addition, different from traditional lenses designed in the spatial domain, our conformal magnifier is defined in the parameter domain: the conformal parameterization is first calculated and stored, and then apply texture mapping or volume rendering based on the precomputed parameters. Therefore, our system can be easily embedded into various graphics or visualization frameworks, including the route, map, surface model, and 3D volumetric data. With the support of experimental results and comparisons within various task scenarios, we have demonstrated that our conformal magnifier, as a novel F+C technique, has great potentials for the volume graphics and visualization applications.

Limitations and future work. Our method can well preserve local angles and achieve a smooth transition with minimal visual distortions. However, visual distortions are not only due to the deviation of angles. The size variation of neighboring regions may also introduce distortions. Fortunately, according to the theory of human central vision, we are sensitive to sharp transitions of intensity or color, which are usually detected as local features and are well preserved by our framework. Meanwhile, using a smooth mesh model as the conformal magnifier, the magnification ratio varies continuously. Therefore, the size variation of neighboring regions is smoothly changing without any obvious difference. With the fact that only a small area in the center of the retina contains a rich collection of cone cells, the user usually concentrates on the well-preserved local shape/feature of interest and disregards the area distortion of surrounding contexts. This means that the distortion caused by the size variation of neighboring regions is not disturbing to the user using our conformal magnifier. In addition, because our system achieves real-time performance, the user can quickly move the conformal magnifier in the neighboring areas of interest to reach the accurate perception of features.

Another limitation of our framework is how to generate smooth and grid-unified mesh models, which is a key factor to produce F+C visualizations with minimal distortion and smooth transition. Therefore, some specified filters or blending algorithms are required to further smooth the transition region of magnifier models to obtain high-quality results. Also, the computational speed of conformal mapping, although not slow, still needs to be improved for interactive magnification operations. We plan to further accelerate the calculation of conformal mapping and to incorporate new rendering methods for the high performance and resolution using GPU.

ACKNOWLEDGMENTS

This work has been partially supported by US National Science Foundation (NSF) grants EAGER-1050477, CCF-0702699, and IIS-0916235. The authors would also like to thank the Stony Brook Hospital for the medical data sets and professional evaluation.

REFERENCES

[1] F. Bernardini, J. Mittleman, H. Rushmeier, C. Silva, and G. Taubin, "The Ball-Pivoting Algorithm for Surface Reconstruction," *IEEE Trans. Visualization and Computer Graphics,* vol. 5, no. 4, pp. 349-359, Oct.-Dec. 1999.

[2] E.A. Bier, M.C. Stone, K. Pier, W. Buxton, and T.D. Derose, "Toolglass and Magic Lenses: The See-through Interface," *Proc. SIGGRAPH,* pp. 73-80, 1993.

[3] J. Brosz, F.F. Samavati, M.T.C. Sheelagh, and M.C. Sousa, "Single Camera Flexible Projection," *Proc. Fifth Int'l Symp. Nonphotorealistic Animation and Rendering (NPAR '07),* pp. 33-42, 2007.

[4] M.S.T. Carpendale, D.J. Cowperthwaite, and F.D. Fracchia, "Extending Distortion Viewing from 2D to 3D," *IEEE Computer Graphics and Applications,* vol. 17, no. 4, pp. 42-51, July 1997.

[5] M.S.T. Carpendale, J. Ligh, and E. Pattison, "Achieving Higher Magnification in Context," *Proc. 17th Ann. ACM Symp. User Interface Software and Technology (UIST '04),* pp. 71-80, 2004.

[6] M.S.T. Carpendale and C. Montagnese, "A Framework for Unifying Presentation Space," *Proc. 14th Ann. ACM Symp. User Interface Software and Technology (UIST '01),* pp. 61-70, 2001.

[7] M.S.T. Carpendale, M. Sheelagh, T. Carpendale, D.J. Cowperthwaite, and F.D. Fracchia, "Multi-Scale Viewing," *Proc. SIGGRAPH,* pp. 149-152, 1996.

[8] B. Chow, "The Ricci Flow on the 2-Sphere," *J. Differential Geometry,* vol. 33, no. 2, pp. 325-334, 1991.

[9] B. Chow and F. Luo, "Combinatorial Ricci Flows on Surfaces." *J. Differential Geometry,* vol. 63, no. 1, pp. 97-129, 2003.

[10] M. Cohen, K. Brodlie, and N. Phillips, "The Volume in Focus: Hardware Assisted Focus and Context Effects for Volume Visualization," *Proc. ACM Symp. Applied Computing (SAC '08),* pp. 1235-1239, 2008.

[11] H.M. Farkas and I. Kra, *Riemann Surfaces.* Springer, 2004.

[12] J.D. Fekete and C. Plaisant, "Interactive Information Visualization of a Million Items," *Proc. IEEE Symp. Information Visualization,* pp. 117-124, 2002.

[13] A. Formella and J. Keller, "Generalized Fisheye Views of Graphs," *Proc. Symp. Graph Drawing (GD '95),* pp. 242-253, 1995.

[14] E. Gansner, Y. Koren, and S. North, "Topological Fisheye Views for Visualizing Large Graphs," *Proc. IEEE Symp. Information Visualization (INFOVIS '04),* pp. 175-182, 2004.

[15] D.X. Gu, W. Zeng, F. Luo, and S.-T. Yau, "Numerical Computation of Surface Conformal Mappings," *Computational Methods and Functional Theory,* vol. 11, no. 2, pp. 747-787, 2011.

[16] H.W. Guggenheimer, *Differential Geometry.* Dover Publications, 1977.

[17] R.S. Hamilton, "Three Manifolds with Positive Ricci Curvature," *J. Differential Geometry,* vol. 17, pp. 255-306, 1982.

[18] W. Hong, F. Qiu, and A. Kaufman, "A Pipeline for Computer Aided Polyp Detection," *IEEE Trans. Visualization and Computer Graphics,* vol. 12, no. 5, pp. 861-868, Sept./Oct. 2006.

[19] M. Jin, J. Kim, F. Luo, and X. Gu, "Discrete Surface Ricci Flow," *IEEE Trans. Visualization and Computer Graphics,* vol. 14, no. 5, pp. 1030-1043, Sept. 2008.

[20] P. Karnick, D. Cline, S. Jeschke, A. Razdan, and P. Wonka, "Route Visualization Using Detail Lenses," *IEEE Trans. Visualization and Computer Graphics,* vol. 16, no. 2, pp. 235-247, Mar./Apr. 2010.

[21] T.A. Keahey, "The Generalized Detail-in-Context Problem," *Proc. IEEE Symp. Information Visualization (INFOVIS '98),* pp. 44-51, 1998.

[22] T.A. Keahey, "Getting along: Composition of Visualization Paradigms," *Proc. IEEE Symp. Information Visualization (INFOVIS '01),* pp. 37-40, 2001.

[23] T.A. Keahey and E.L. Robertson, "Nonlinear Magnification Fields," *Proc. IEEE Symp. Information Visualization,* pp. 51-58, 1997.

[24] E. LaMar, B. Hamann, and K.I. Joy, "A Magnification Lens for Interactive Volume Visualization," *Proc. Ninth Pacific Conf. Computer Graphics and Applications (PG '01),* pp. 223-232, 2001.

[25] Y.K. Leung and M.D. Apperley, "A Review and Taxonomy of Distortion-Oriented Presentation Techniques," *ACM Trans. Computer-Human Interaction,* vol. 1, no. 2, pp. 126-160, 1994.

[26] T. Munzner, "H3: Laying Out Large Directed Graphs in 3D Hyperbolic Space," *Proc. IEEE Symp. Information Visualization,* pp. 2-8, 1997.

[27] T. Munzner, F. Guimbretière, S. Tasiran, L. Zhang, and Y. Zhou, "Treejuxtaposer: Scalable Tree Comparison Using Focus+Context with Guaranteed Visibility," *ACM Trans. Graphics,* vol. 22, pp. 453-462, 2003.

[28] E. Pietriga and C. Appert, "Sigma Lenses: Focus-Context Transitions Combining Space, Time and Translucence," *Proc. 26th Ann. SIGCHI Conf. Human Factors in Computing Systems (CHI '08),* pp. 1343-1352, 2008.

[29] E. Pietriga, O. Bau, and C. Appert, "Representation-Independent in-Place Magnification with Sigma Lenses," *IEEE Trans. Visualization and Computer Graphics,* vol. 16, no. 3, pp. 455-467, May 2010.

[30] H. Qu, H. Wang, W. Cui, Y. Wu, and M.-Y. Chan, "Focus+Context Route Zooming and Information Overlay in 3D Urban Environments," *IEEE Trans. Visualization and Computer Graphics,* vol. 15, no. 6, pp. 1547-1554, Nov. 2009.

[31] J. Ruppert, "A Delaunay Refinement Algorithm for Quality 2-Dimensional Mesh Generation," *J. Algorithms,* vol. 18, no. 3, pp. 548-585, 1995.

[32] R. Schoen and S.-T. Yau, *Lectures on Harmonic Maps.* Int'l Press, pp. 187-241, 1997.

[33] K. Shi, P. Irani, and B. Li, "An Evaluation of Content Browsing Techniques for Hierarchical Space-Filling Visualizations," *Proc. IEEE Symp. Information Visualization (INFOVIS '05),* pp. 11-18, 2005.

[34] J. Slack and T. Munzner, "Composite Rectilinear Deformation for Stretch and Squish Navigation," *IEEE Trans. Visualization and Computer Graphics,* vol. 12, no. 5, pp. 901-908, Sept. 2006.

[35] R. Spence and M. Apperley, "Bifocal Display," http://www.interaction-design.org/encyclopedia/bifocal-display.html, 2012.

[36] M. Spindler, M. Bubke, T. Germer, and T. Strothotte, "Camera Textures," *Proc. Conf. Computer Graphics and Interactive Techniques,* pp. 295-302, 2006.

[37] J. Stasko and E. Zhang, "Focus+Context Display and Navigation Techniques for Enhancing Radial, Space-Filling Hierarchy Visualizations," *Proc. IEEE Symp. Information Visualization (INFOVIS '00),* pp. 57-64, 2000.

[38] S. Stegmaier, M. Strengert, T. Klein, and T. Ertl, "A Simple and Flexible Volume Rendering Framework for Graphics-Hardware-Based Raycasting," *Proc. Fourth Int'l Workshop Volume Graphics,* pp. 187-241, 2006.

[39] T. Tenev and R. Rao, "Managing Multiple Focal Levels in Table Lens," *Proc. IEEE Symp. Information Visualization,* pp. 59-66, 1997.

[40] W.P. Thurston, *Geometry and Topology of Three-Manifolds.* Princeton Univ., 1980.

[41] M. Toyoda and E. Shibayama, "Hyper Mochi Sheet: A Predictive Focusing Interface for Navigating and Editing Nested Networks through a Multi-Focus Distortion-Oriented View," *Proc. SIGCHI Conf. Human Factors in Computing Systems (CHI '99),* pp. 504-511, 1999.

[42] M. Trapp, T. Glander, H. Buchholz, and J. Dollner, "3D Generalization Lenses for Interactive Focus+Context Visualization of Virtual City Models," *Proc. 12th Int'l Conf. Information Visualisation (IV '08),* pp. 356-361, 2008.

[43] L. Wang, Y. Zhao, K. Mueller, and A. Kaufman, "The Magic Volume Lens: An Interactive Focus+Context Technique for Volume Rendering," *Proc. IEEE Visualization,* pp. 367-374, 2005.

[44] Y.-S. Wang, T.-Y. Lee, and C.-L. Tai, "Focus+Context Visualization with Distortion Minimization," *IEEE Trans. Visualization and Computer Graphics,* vol. 14, no. 6, pp. 1731-1738, Nov./Dec. 2008.

[45] Y.-S. Wang, C. Wang, T.-Y. Lee, and K.-L. Ma, "Feature-Preserving Volume Data Reduction and Focus+Context Visualization," *IEEE Trans. Visualization and Computer Graphics,* vol. 17, no. 2 pp. 171-181, Feb. 2011.

[46] J. Yang, M.O. Ward, E.A. Rundensteiner, and A. Patro, "Interring: A Visual Interface for Navigating and Manipulating Hierarchies," *J. Information Visualization,* vol. 2, no. 1, pp. 16-30, Mar. 2003.

[47] Y. Yang, J.X. Chen, and M. Beheshti, "Nonlinear Perspective Projections and Magic Lenses: 3D View Deformation," *IEEE Computer Graphics and Applications,* vol. 25, no. 1, pp. 76-84, Jan./Feb. 2005.

[48] H. Ziegler and D.A. Keim, "Copernicus: Context-Preserving Engine for Route Navigation with Interactive User-Modifiable Scaling," *Computer Graphics Forum,* vol. 27, no. 3, pp. 927-934, 2008.

Xin Zhao received the BS degree in computer science from Zhongshan University, Guangzhou, China in 2007. She is currently working toward the PhD degree. She is a research assistant in the Department of Computer Science, Stony Brook University, Stony Brook, New York. Her research interests include F+C visualization and lens design, feature-guided deformation, and animation.

Wei Zeng received the BS and MS degrees in computer science from Shandong University of China in 2002 and 2005, respectively, and the PhD degree from the Institute of Computing Technology, Chinese Academy of Sciences in 2008. She is a postdoctoral research associate in the Department of Computer Science, Stony Brook University, Stony Brook, New York. Her research interests include computational conformal and quasi-conformal geometry, and shape analysis, including surface matching, registration, tracking, and recognition. She is a member of the IEEE and IEEE Computer Society.

Xianfeng David Gu received the PhD degree in computer science from Harvard University in 2003. He is an associate professor of computer science and the director of the 3D Scanning Laboratory in the Department of Computer Science in the State University of New York at Stony Brook University. His research interests include computer graphics, vision, geometric modeling, and medical imaging. His major works include global conformal surface parameterization in graphics, tracking and analysis of facial expression in vision, manifold splines in modeling, brain mapping, and virtual colonoscopy in medical imaging, and computational conformal geometry. He won the US National Science Foundation CAREER Award in 2004. He is a member of the IEEE and IEEE Computer Society.

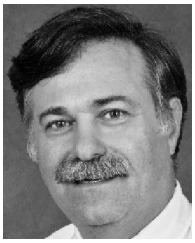

Arie E. Kaufman received the BS degree in 1969 in mathematics and physics from the Hebrew University of Jerusalem, Israel, the MS degree in 1973 in computer science from the Weizmann Institute of Science, Rehovot, Israel, and the PhD degree in 1977 in computer science from the Ben-Gurion University, Israel. He is a distinguished professor and the chair of the Computer Science Department, the chief scientist of the Center of Excellence in Wireless and Information Technology (CEWIT), and the director of the Center for Visual Computing (CVC) at Stony Brook University (Aka State University of New York at Stony Brook). He is the recipient of IEEE Visualization Career Award in 2005. He further received the IEEE Outstanding Contribution Award (1995), ACM Service Award (1998), IEEE CS Meritorious Service Award (1999), member of the European Academy of Sciences (since 2002), State of New York Entrepreneur Award (2002), IEEE Harold Wheeler Award (2004), and State of New York Innovative Research Award (2005). He was the founding editor-in-chief of *IEEE Transactions on Visualization and Computer Graphics* (TVCG), 1995-1998. He has been the cofounder, papers/program cochair, and a member of the steering committee of IEEE Visualization Conferences; co-founder/chair of Volume Graphics Workshops; cochair for Eurographics/SIGGRAPH Graphics Hardware Workshops, and the Papers/Program cochair for ACM Volume Visualization Symposia. He previously chaired and is currently the director of IEEE CS Technical Committee on Visualization and Graphics. He has conducted research and consulted for more than 40 years specializing in volume visualization, graphics architectures, algorithms, and languages, virtual reality, user interfaces, medical imaging, and their applications. He is a fellow of the IEEE, IEEE Computer Society, and ACM. For more information, see http://www.cs.sunysb.edu/~ari.

Wei Xu received the BS and MS degrees in computer science from Zhejiang University in 2004 and 2006. She is currently working toward the PhD degree. She is a research assistant in the Department of Computer Science, Stony Brook University, Stony Brook, New York. Her research interests include regularization and parameter learning for low-dose CT reconstruction with GPU acceleration, low-level image processing for artifact reduction, visualization, and visual analytics.

Klaus Mueller received the MS degree in biomedical engineering and the PhD degree in computer science, both from The Ohio State University. He is currently an associate professor in the Computer Science Department at Stony Brook University, where he also holds coappointments in the Biomedical Engineering and Radiology Departments. His current research interests include computer and volume graphics, visualization, visual analytics, medical imaging, and computer vision. He won the US National Science Foundation CAREER Award in 2001 and the SUNY Chancellor Award for Excellence in Scholarship and Creative Activity in 2011. He served as the cochair at various conferences, such IEEE Visualization, Volume Graphics Symposium, and the Fully 3D Workshop on High-Performance Image Reconstruction. He has authored and coauthored more than peer-reviewed 140 journal and conference papers, and he has participated in 15 tutorials at international conferences on various topics in visualization and medical imaging. He is a senior member of the IEEE and IEEE Computer Society. For more information, see http://www.cs.sunysb.edu/~mueller.